Jahn–Teller energy, bandwidth, and Curie temperature in Ni/Co-doped $LaMnO_3$

2005 J. Phys.: Condens. Matter 17 6507

(http://iopscience.iop.org/0953-8984/17/41/020)

INSTITUTE OF PHYSICS PUBLISHING JOURNAL OF PHYSICS: CONDENSED MATTER

J. Phys.: Condens. Matter **17** (2005) 6507–6517 doi:10.1088/0953-8984/17/41/020

Jahn–Teller energy, bandwidth, and Curie temperature in Ni/Co-doped $LaMnO_3$

F L Tang and X Zhang[1]

The Key Laboratory of Advanced Materials, Department of Materials Science and Engineering, Tsinghua University, Beijing 100084, People's Republic of China

E-mail: xzzhang@tsinghua.edu.cn

Received 27 June 2005, in final form 30 August 2005
Published 30 September 2005
Online at stacks.iop.org/JPhysCM/17/6507

Abstract

The Jahn–Teller energy, bandwidth and Curie temperature T_C of $LaMn_{1-x}M_xO_3$ (M = Ni, Co, $0 \leqslant x \leqslant 0.208$) are calculated using the atomic simulation technique. The simulated Jahn–Teller energy is in agreement with the data deduced from experimental results. It is found that there is a strong relation between the doping-introduced strains and T_C. The calculated T_C agrees well with experimental results.

1. Introduction

The manganese-based magnetoresistive oxides have been the subjects of intense investigations due to their rich underlying physics and potential application [1–3]. It has been found that the magnetic-transport phase diagram closely depends on the structural transition [4, 5]. Moreover, the bandwidth and Jahn–Teller energy in these compounds are affected by their crystal structure [6–8]. The relation between lattice strains, doping ion size, Jahn–Teller distortion energy E_{JT}, bandwidth W and Curie temperature T_C in doped manganites has been studied [9–11].

Some theoretical [12] and experimental [13] results indicated that T_C exhibits strong correlations with substrate-introduced strains in manganite films, which contain bulk and Jahn–Teller (JT) components. In thickness $t > 20$ nm $Pr_{0.67}Sr_{0.33}MnO_3$ films on different substrates [14], the lattice transition effect on T_C analysis led to an interesting suggestion that the biaxial tensile strain affected the zero-field resistance peak temperature T_P more than the biaxial compressive strain with a relatively large JT contribution.

As mentioned above, the effect of structure transition on T_C of La-site doped $LaMnO_3$ has been studied and most of these works have been qualitatively done. To our knowledge, little work had been carried out on the variation of lattice strains and E_{JT} and their effect on T_C in doped $LaMnO_3$. Moreover, it is necessary to consider the effect of lattice changes on T_C. Also, little work has been done in Mn-site doped $LaMnO_3$. In this work, we used the atomic simulation technique to study the crystal structural transition, the variation of E_{JT} in

[1] Author to whom any correspondence should be addressed.

$LaMn_{1-x}M_xO_3$ (M = Ni, Co, $0 \leqslant x \leqslant 0.208$), and, in particular, the effect of the lattice strains on T_C.

2. Method

The crystal structure of a material at a given temperature and pressure can be predicted by minimizing its free energy by adjusting the cell volume and atomic positions until the net pressure or stress is zero. The pressure P is simply the derivative of the free energy F with respect to volume V. Thus for a cubic material

$$P = \mathrm{d}F/\mathrm{d}V. \tag{1}$$

Calculating the free energy at a given volume and then recalculating it after making a small adjustment to the cell volume $\mathrm{d}V$ determines the pressure. The problem becomes slightly more complicated for non-cubic material because the volume will not expand isotropically. For these systems we have to consider six different strain components ε_j. However, the same approach is used except that a small strain is applied in each of the six senses, and a pressure corresponding to the derivative of the free energy for each component is calculated assuming the thermal contribution to the pressure is isotropic:

$$P_j = \frac{1}{V}\frac{\mathrm{d}F}{\mathrm{d}\varepsilon_j}, \tag{2}$$

where V is the unit cell volume. During the iterative procedure a constant volume energy minimization is performed. Hence each time the cell volume is modified all atomic positions are adjusted so that they remain at a potential energy minimum. Thus by minimizing to constant pressure and including the vibrational component of the free energy the crystal structure at a given temperature and pressure can be predicted. Detailed discussions of these methodologies are given in [15, 16]. Some simulation codes, based on the use of lattice dynamics in the quasiharmonic approximation, allow the optimization of unit cells with several hundred atoms and for hundreds of configurations. Results of these calculations are already available [17]. More recently, several works using configurational lattice dynamics to study disordered solids have been published [18, 19].

Our simulation is based on the shell model generalization of the Born model of a solid, by which some properties of SiO_2, $MgSiO_3$ [15], and superconductors [20–22] have been successfully investigated. Short-range interaction forces are represented with Buckingham potential

$$V(r) = A\exp(-r/\rho) - Cr^{-6}, \tag{3}$$

where A, ρ, and C are constants, and r is the distance between two atoms. The potential parameters are obtained by an empirical method, known as the 'relaxed' fitting approach. The crystal structure is relaxed to zero strain for every evaluation of the sum of squares, using the difference between observed and calculated structural parameters. In each step in the fitting the minimization was started from the experimental structure to avoid the possibility that the fit becomes trapped in an undesirable local minimum in potential of geometry space. It should be stressed that the reliability of the simulations depends on the validity of the potential model used in the calculation, and the latter is assessed primarily by its ability to reproduce experimental crystal properties. Potential parameters used for calculation in this work are obtained from [23] and given in table 1. And these potentials can reproduce the structure of $LaMnO_3$ excellently.

Some experiments have confirmed that Ni and Co ions in low-doped $LaMnO_3$ are divalent [24–27]. In this work Ni and Co ions are assigned with 2+ charge state. Their potential parameters are obtained from [22] and given in table 2.

Table 1. Potential parameters of $LaMnO_3$ and Mn^{4+}. In the superlattice, O atoms in the La planes which are perpendicular to the *b* direction are labelled as O1, and O atoms in the Mn planes which are perpendicular to the *b* direction are labelled as O2.

	Short-range interaction		
	A (eV)	ρ (Å)	C (eV Å^6)
$O1^{2-}$–$O1^{2-}$	22 764.3000	0.1490	43.0
$O2^{2-}$–$O2^{2-}$	22 764.3000	0.1490	43.0
$O1^{2-}$–$O2^{2-}$	22 764.3000	0.1490	43.0
La^{3+}–$O1^{2-}$	2 800.0828	0.3274	0.0
La^{3+}–$O2^{2-}$	23 533.3281	0.2447	0.0
Mn^{3+}–$O1^{2-}$	8 474.5750	0.2392	0.0
Mn^{3+}–$O2^{2-}$	344.0376	0.4431	0.0
Mn^{4+}–$O1^{2-}$	16 526.0604	0.2218	0.0
Mn^{4+}–$O2^{2-}$	16 741.0424	0.2217	0.0
	Shell-model parameters		
Species	Y (e)	K (eV Å^{-2})	
La^{3+}	−0.250	145.0	
Mn^{3+}	3.000	95.0	
Mn^{4+}	4.000	95.0	
$O1^{2-}$	−2.389	42.0	
$O2^{2-}$	−2.389	42.0	

Table 2. Potential parameters of Ni^{2+} and Co^{2+}.

	Short-range interaction		
	A (eV)	ρ (Å)	C (eV Å^6)
Ni^{2+}–O^{2-}	1582.5	0.2882	0.0
Co^{2+}–O^{2-}	1491.7	0.2951	0.0
	Shell-model parameters		
Species	Y (e)	K (eV Å^{-2})	
Ni^{2+}	3.344	93.7	
Co^{2+}	3.503	110.5	

3. Results and discussion

3.1. Structural data

The parent superlattice used in our simulation consists of 24 $LaMnO_3$ unit cells. At every doping density, about 20–300 doping configurations are simulated. We calculated the average cell volume of these configurations, and found that the average volumes decrease with the doping content increase (figure 1). This result is in agreement with the experimental result, especially in the case of Ni doping.

The variations of the lattice parameters of $LaMn_{1-x}M_xO_3$ ($0 \leqslant x \leqslant 0.208$) with Ni or Co doping were calculated (figure 2). Concerning the three lattice parameters a, b, and c (in the symmetry of *pnma*), we assigned the maximum one as the lattice parameter b, the minimum one as the lattice parameter c, and the one with intermediate length as the lattice parameter

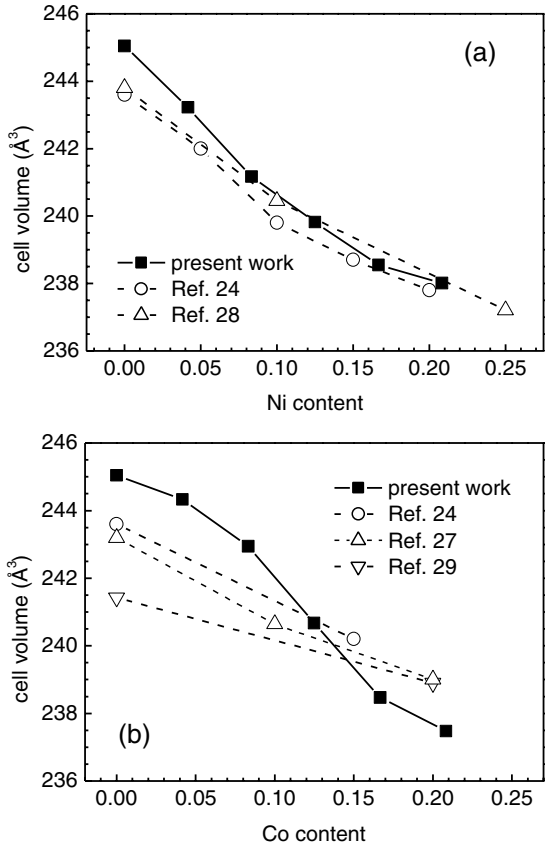

Figure 1. Comparison of calculated and experimental cell volume of (a) $LaMn_{1-x}Ni_xO_3$ ($0 \leqslant x \leqslant 0.208$) and (b) $LaMn_{1-x}Co_xO_3$ ($0 \leqslant x \leqslant 0.208$).

a. It is found that as the doping content increases the calculated lattice parameter a decreases significantly, b increases a little, but c almost remains unchanged (figure 2(a)). Our calculation results agree with the experimental data.

Our simulations were performed at 0 K whereas the experimental results were obtained from bulk or powder samples measured at ambient temperature [24, 27–29]. Can calculated lattice parameters represent correctly the experimental lattice parameters? To our knowledge, little experimental work has been done on the relationship between lattice variations and temperature in Ni- or Co-doped $LaMnO_3$. It was reported [30] that the maximum lattice displacement of un-doped $LaMnO_3$ was about 0.02 Å when temperature changed from about 0 to 200 K, and the maximum change in lattice parameters of $La_{0.52}Y_{0.15}Ca_{0.33}MnO_3$ was about 0.01 Å when temperature changed from about 0 to 185 K [31]. But the maximum change in lattice parameters due to doping in Ni- or Co-doped manganites was about 0.2 Å [24, 27–29], about ten times more than that caused by temperature. In comparison with the doping effect, the temperature effect on lattice parameters is small and it can be neglected. Hence our simulated structural change may represent correctly the real structural change.

In the case of Ni doping, La–O and Mn–O bond lengths, Mn–O–Mn angle and structural factor were calculated (figure 3). With the increase of doping content x ($0 \leqslant x \leqslant 0.208$), La–O and Mn–O2 bond lengths are found to decrease, but Mn–O1 bond length is almost unchanged.

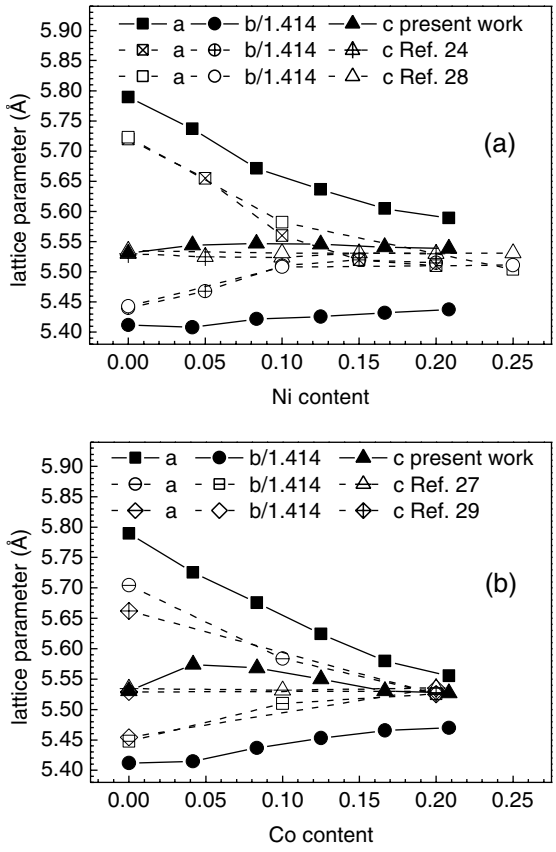

Figure 2. Comparison of calculated and experimental lattice parameters of (a) $LaMn_{1-x}Ni_xO_3$ ($00 \leqslant x \leqslant 0.208$) and (b) $LaMn_{1-x}Co_xO_3$ ($0 \leqslant x \leqslant 0.208$).

In this work, the structural factor τ is defined as $\tau = \sqrt{2}b/(a+c)$ [32]. With increasing of the doping content, the τ increases and Mn–O–Mn bond angles increase from 154° to 157.5°, indicating the lattice distortion decreases. The structural changes in the case of Co doping (figure 4) are similar to that of Ni doping. But with the increase of doping content Mn–O1 bond length decreases whereas Mn–O2 bond length increases. It is also noted that the change in structural factor in the case of Co doping is larger than that in the case of Ni doping.

3.2. Bandwidth and Jahn–Teller energy

For perovskite compounds with general formula ABO_3, it is a straightforward result from the tight-binding approximation that the O 2p-like bandwidth W depends on both the B–O–B and B–O bond lengths, through the overlap integrals between the 3d orbital of the metal ion B and the 2p orbital of the O anion. The following empirical formula has been used to describe this double dependence [7]: to a first approximation, the bandwidth W of manganites can be calculated using [6, 7, 11]

$$W \propto \frac{\cos\delta}{d^{3.5}}, \tag{4}$$

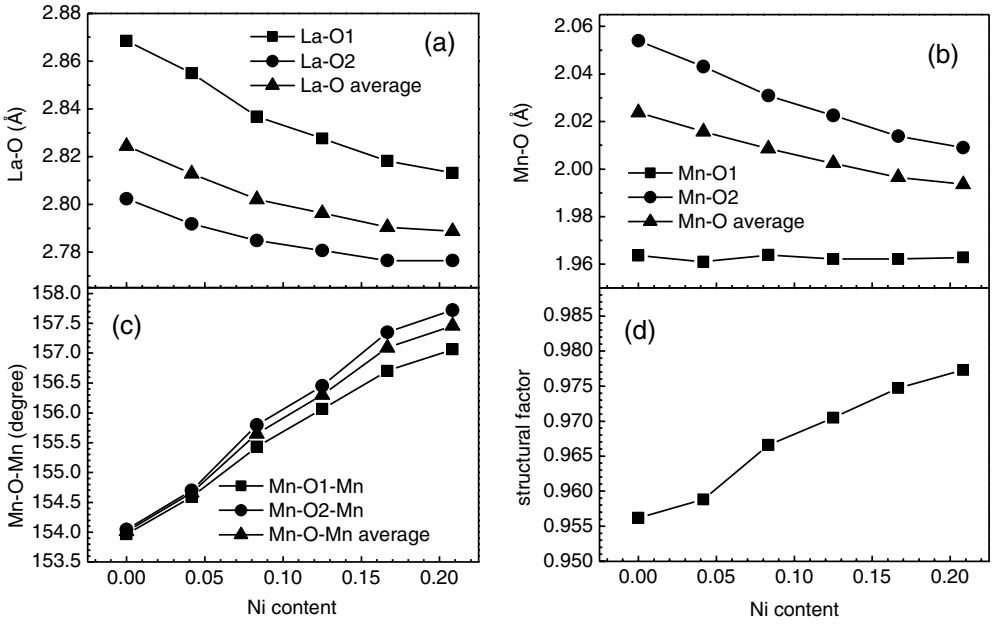

Figure 3. Calculated La–O (a) and Mn–O (b) bond length, Mn–O–Mn bond angle (c) and structural factor (d) of $LaMn_{1-x}Ni_xO_3$ ($0 \leqslant x \leqslant 0.208$).

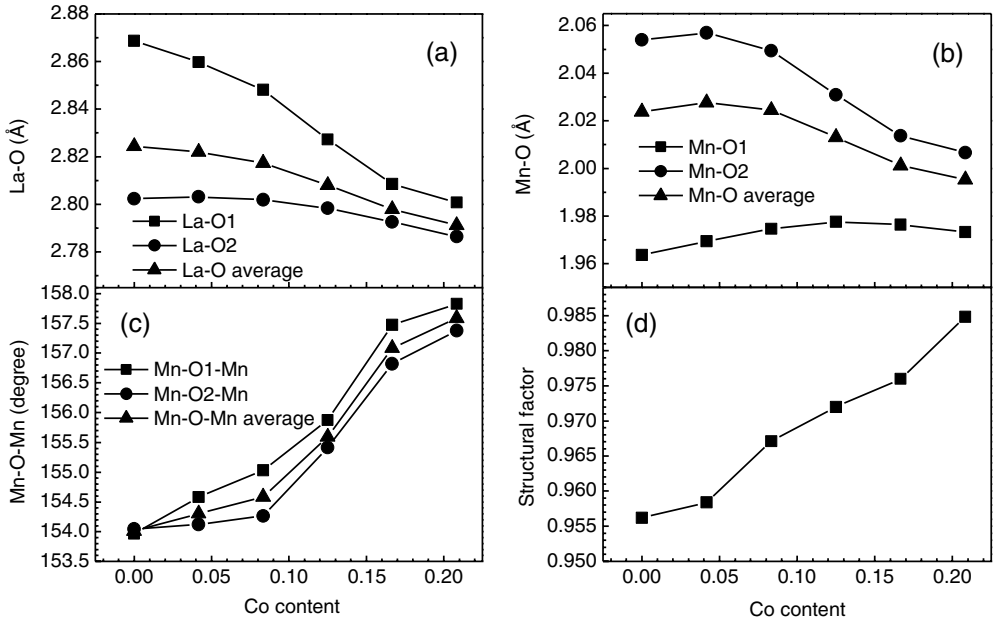

Figure 4. Calculated La–O (a) and Mn–O (b) bond length, Mn–O–Mn bond angle (c) and structural factor (d) of $LaMn_{1-x}Co_xO_3$ ($0 \leqslant x \leqslant 0.208$).

where δ is tilt angle, defined as $(180 - \phi)/2$, ϕ is Mn–O–Mn bond angle, and d is Mn–O bond length. Our calculation shows that with increase of doping content the bandwidth of

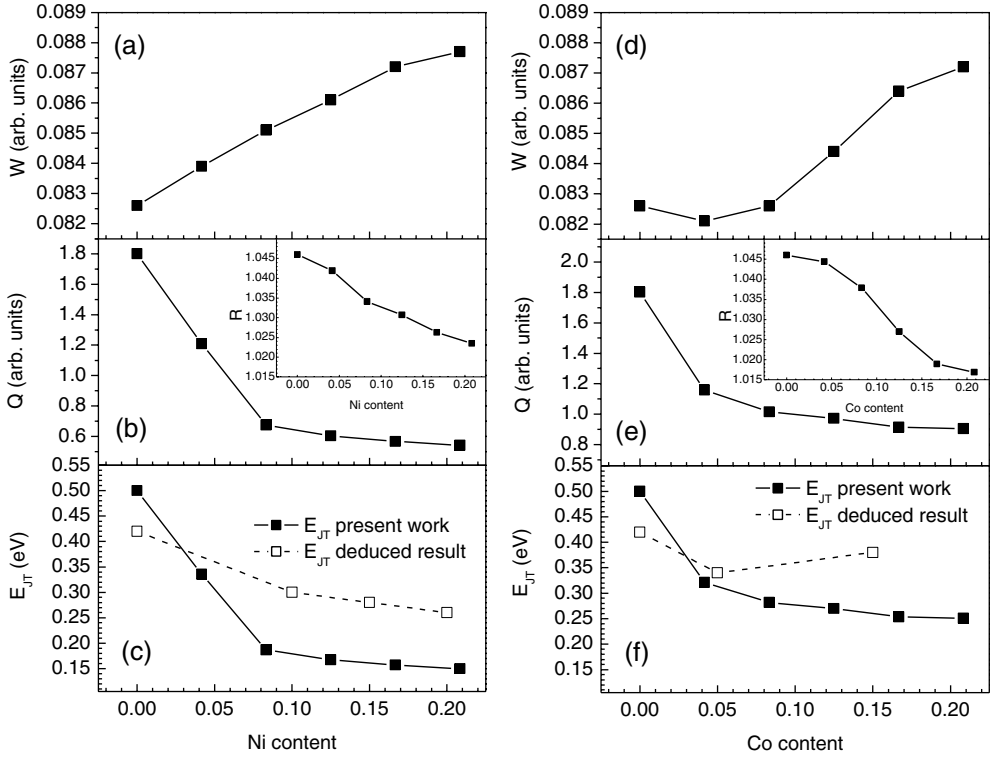

Figure 5. Calculated bandwidth W (a), Jahn–Teller distortion Q (b) and R (inset of (b); R has been defined as a crude representation of Q in the text), and Jahn–Teller energy E_{JT} (c) of $LaMn_{1-x}Ni_xO_3$ ($0 \leqslant x \leqslant 0.208$). Calculated bandwidth W (d), Jahn–Teller distortion Q (e) and R (inset of (e)), and Jahn–Teller energy E_{JT} (f) of $LaMn_{1-x}Co_xO_3$ ($0 \leqslant x \leqslant 0.208$). The deduced E_{JT} is the E_{JT} deduced from the experimental result.

$LaMn_{1-x}Ni_xO_3$ increases whereas the bandwidth of $LaMn_{1-x}Co_xO_3$ firstly decreases then increases (figures 5(a) and (d)).

Taking into account only lattice distortions, Jahn–Teller energy E_{JT} can be presented using the following formula [8]:

$$\frac{E_{JT}}{N_{Mn}} = -\frac{1}{2}\sqrt{\frac{3}{2}}\lambda\left[\sqrt{(Q_{2u}+Q_{2s})^2+(Q_{3u}+Q_{3s})^2}+\sqrt{(Q_{2u}-Q_{2s})^2+(Q_{3u}-Q_{3s})^2}\right], \quad (5)$$

where N_{Mn} is the number of Mn ions in the superlattice, and λ is the Jahn–Teller coupling constant. In equation (5),

$$Q_{2u} = \frac{a_0}{\sqrt{2}}(e_{xx}-e_{yy}), \quad (6)$$

$$Q_{3u} = \frac{a_0}{\sqrt{6}}(2e_{zz}-e_{xx}-e_{yy}), \quad (7)$$

$$Q_{2s} = \frac{a_0}{\sqrt{2}}(v_{sx}-v_{sy}), \quad (8)$$

$$Q_{3s} = \frac{a_0}{\sqrt{6}}(2v_{sz}-v_{sx}-v_{sy}), \quad (9)$$

where a_0 is the lattice parameter of the ideal cubic perovskite structure. In this work $a_0 = (abc/4)^{1/3}$ as our simulated structure has symmetry $pnma$. In equations (6) and (7), e_{jj} is

the diagonal component of the conventional strain tensor referred to the ideal cubic perovskite lattice. In equations (8) and (9) $v_i^a = u_i^a - u_{i-\hat{a}}^a$, where u_i^a and $u_{i-\hat{a}}^a$ are displacements of the two O ions in the MnO_6 octahedron along the a direction. The details about the formulas can be found in [1, 8] and [33]. The Jahn–Teller distortion of an octahedron Q is defined as

$$Q = \sqrt{(Q_{2u} + Q_{2s})^2 + (Q_{3u} + Q_{3s})^2} + \sqrt{(Q_{2u} - Q_{2s})^2 + (Q_{3u} - Q_{3s})^2}, \quad (10)$$

where Q_{2s} and Q_{3s} can be easily calculated from the coordinates of six O atoms, and Q_{2u}, Q_{3u} from lattice parameters. The Jahn–Teller distortion of a configuration is calculated by averaging the Q of every octahedron in the superlattice. The Q at a specific doping level is calculated by averaging the Q of every configuration considered. It is found that the calculated Jahn–Teller distortion Q decreases with increase of x (figure 5). When doping content changes from 0 to 0.208, the Q of $LaMn_{1-x}Ni_xO_3$ decreases by about 70% whereas the Q of $LaMn_{1-x}Co_xO_3$ decreases by about 50% (figures 5(b) and (e)).

There are several ways to suppress Jahn–Teller distortion [34]: substitution of La^{3+} by divalent ion, self-doping and applying a hydrostatic pressure. Our simulation result that Jahn–Teller distortion Q decreases with increase of Ni^{2+} or Co^{2+} doping content indicates that there is possibly a fourth way to suppress Jahn–Teller distortion, namely, substitution of Mn^{3+} by divalent ions, at least, by Co^{2+} or Ni^{2+}.

A crude presentation of Jahn–Teller distortion [34] has been defined as $R = l/s$, where l is the long Mn–O bond length and s is the short Mn–O bond length. Our calculation shows that when doping content changes from 0 to 0.208, the R of $LaMn_{1-x}Ni_xO_3$ decreases by about 2% whereas the R of $LaMn_{1-x}Co_xO_3$ decreases by about 3% (inset of figures 5(b) and (e)). Comparing with the results of Q, the R is too crude to describe the Jahn–Teller distortion Q.

It was reported that the Jahn–Teller energy E_{JT} of $LaMnO_3$ was about 0.5 eV [9, 35]. We used 0.5 eV as the value of E_{JT} for un-doped $LaMnO_3$. The values of E_{JT} of doped $LaMnO_3$ can be calculated using equations (5) and (10) and are shown in figures 5(c) and (f). It is found that when doping content changes from 0 to 0.208 the E_{JT} of $LaMn_xNi_{1-x}O_3$ decreases by about 70% and the E_{JT} of $LaMn_xCo_{1-x}O_3$ decreases by about 50%.

It was found that the E_{JT} can also be estimated using the experimental activation energy E_A [24] in $LaMn_{1-x}Ni_xO_3$ ($0 \leqslant x \leqslant 0.2$) and $LaMn_{1-x}Co_xO_3$ ($0 \leqslant x \leqslant 0.15$), by the formulas of $E_{JT} \approx E_P$ [9] and $E_P \approx 2E_A$ [10]. This estimated E_{JT} is called deduced E_{JT} in this paper and shown in figures 5(c) and (f). The qualitative agreement between the deduced E_{JT} and our calculated E_{JT} indicates that our calculated E_{JT} are reasonable.

3.3. Curie temperature

T_C is an important property parameter for doped manganites, as their CMR effect always takes place near T_C. To our knowledge, there have been at least two influential methods for discussing dependence of T_C on lattice transition in the CMR materials.

One method took into account the substrate-introduced strain effect on T_C in manganite films. Millis *et al* [12] deduced the dependence of T_C on strains by mean field theory and Tsui *et al* [13] rewrote it as

$$T_C(e_b, e_{JT}) = T_C(0,0)(1 - \alpha e_b - \beta e_{JT}^2). \quad (11)$$

In this expansion the respective coefficients for the strains are $\alpha = \frac{1}{T_C(0,0)}\frac{dT_C}{de_b}$, and $\beta = \frac{1}{2T_C(0,0)}\frac{dT_C}{de_{JT}}$. In the films, since the substrate induces an even-parity strain symmetry in the growth plane, the observed three-dimensional strain states by symmetry can be decomposed into a bulk strain,

$$e_b = 2e_{100} + e_{001}, \quad (12)$$

Table 3. Deduced lattice parameters and T_C of Ni-doped $LaMnO_3$. The corresponding strains are listed as percentages.

x	a (Å)	e_{100}	c (Å)	e_{001}	e_b	e_{JT}	T_C (K)
0	4.094	3.85	3.911	−0.80	6.89	−3.79	120
0.042	4.057	2.90	3.921	−0.56	5.24	−2.83	133
0.083	4.011	1.72	3.923	−0.51	2.94	−1.82	146
0.125	3.986	1.10	3.922	−0.53	1.67	−1.33	152
0.167	3.964	0.53	3.919	−0.61	0.45	−0.93	157
0.208	3.953	0.25	3.917	−0.66	−0.15	−0.74	160

Table 4. Deduced lattice parameters and T_C of Co-doped $LaMnO_3$. The corresponding strains are listed as percentages.

x	a (Å)	e_{100}	c (Å)	e_{001}	e_b	e_{JT}	T_C (K)
0	4.094	3.85	3.911	−0.80	6.89	−3.79	120
0.042	4.049	2.69	3.942	−0.02	5.36	−2.22	136
0.083	4.014	1.80	3.938	−0.13	3.47	−1.57	145
0.125	3.977	0.88	3.925	−0.45	1.30	−1.08	154
0.167	3.946	0.08	3.911	−0.81	−0.64	−0.72	162
0.208	3.929	−0.35	3.909	−0.86	−1.57	−0.42	165

and a Jahn–Teller strain,

$$e_{JT} = \sqrt{2/3}(e_{001} - e_{100}), \tag{13}$$

where e_{100} and e_{001} are in-plane and out-of-plane lattice strains in films, which can be calculated from in-plane and out-of-plane lattice parameters, respectively.

However, not only the substrate but also some other external perturbations can cause lattice strains in CMR materials, such as doping, pressure, and even second phase particles. Although the method proposed by Millis and Tsui originated from the relation between substrate-introduced strains and T_C, we simply use equation (11) to discuss the effect of doping-introduced strains on T_C. In order to obtain the doping-introduced strains, firstly we deduce the lattice parameters along (100) and (001) directions by dividing a and c in figure 2 by a factor of 1.414. This deduced parameters fit equation (11) that adopts the pseudocubic symmetry. Then we calculate the strains e_{100} and e_{001} with a bulk value of $a_0 = (abc/4)^{1/3} = 3.943$ Å, which is the simulated parameter of the ideal cubic perovskite structure of the un-doped $LaMnO_3$. Finally, the bulk strain e_b and JT strain e_{JT} are calculated using equations (12) and (13). The deduced lattice parameter a and c, and the values of e_{100}, e_{001}, e_b and e_{JT} of Ni and Co doped $LaMnO_3$ are given in tables 3 and 4, respectively.

Using equation (11) with selected $\alpha = 2.2$, $\beta = 70$ (these are the same as used by Tsui) and $T_C(0, 0) = 160$ K, we calculate T_C (tables 3 and 4) and show the result in figure 6. (For comparison, experimental values of T_C [24, 36–38] are also shown in figure 6. Some experimental T_C shown in figure 6 are deduced from the experimental M_s–T charts with the definition that T_C is the temperature at which dM_s/dT is maximum [37].) For $LaMn_{1-x}Ni_xO_3$, the calculated T_C (see table 3 and figure 6(a)) increases from 120 to 160 K as the doping density x increases from 0 to 0.208. The T_C firstly increases rapidly when $x < 0.1$, and then increases slowly in the range of $0.1 < x \leqslant 0.208$. The calculated curve of T_C is in the middle of the two experimental T_C curves, and has almost the same variation trend as that of the experimental T_C. For $LaMn_{1-x}Co_xO_3$ (see table 4 and figure 6(b)), calculated T_C increases almost linearly from 120 to 165 K as x increases from 0 to 0.208. Our calculated T_C is almost in quantitative

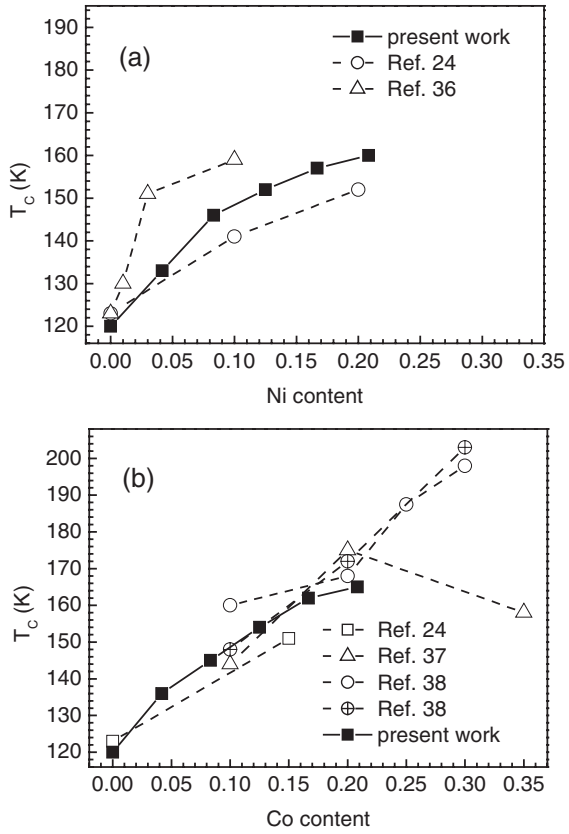

Figure 6. Calculated and experimental T_C of (a) $LaMn_{1-x}Ni_xO_3$ ($0 \leqslant x \leqslant 0.208$) and (b) $LaMn_{1-x}Co_xO_3$ ($0 \leqslant x \leqslant 0.208$).

agreement with the observed T_C. Although equation (11) was deduced for films, figure 6 shows that indeed there is a strong correlation between doping-introduced strains and T_C in Mn-site doped manganites.

We found that the maximum of e_{100} and e_{001} in Ni/Co-doped $LaMnO_3$ is 3.85%, which is just slightly larger than Tsui's value of 3.31% in $La_{0.67}Sr_{0.33}MnO_3$ films [13]. So we can use equation (11) as the equation demands a weak strain condition.

4. Conclusion

The structures of $LaMn_{1-x}M_xO_3$ (M = Ni, Co, $0 \leqslant x \leqslant 0.208$) have been studied using the atomic simulation technique. It is found that as doping content x increases the lattice parameter a decreases and c remains almost unchanged but b slightly increases. It is also found that as doping content x increases the Mn–O–Mn angle increases by about 3.5° and the crystal structure becomes close to cubic. With increasing of doping content x from 0 to 0.208, the bandwidth is found to increase by about 6%, whereas the Jahn–Teller energy decreases from 0.5 to 0.15 eV (Ni doping) or to 0.25 eV (Co doping). Our calculated Jahn–Teller energy is in qualitative agreement with the data deduced from the experimental data. The calculated Curie temperature caused by doping-introduced strains is quantitatively in agreement with the

experimental results, indicating that there is a strong correlation between doping-introduced lattice strains and T_C.

Acknowledgments

The authors are grateful to Y Shao for fruitful discussions. This work was supported by the Ministry of Science and Technology (grant No. TG2000067108).

References

[1] Dagotto E, Hotta T and Moreo A 2001 *Phys. Rep.* **344** 1
[2] Salamon M B and Jaime M 2001 *Rev. Mod. Phys.* **73** 583
[3] Haghiri-Gosnet A-M and Renard J-P 2003 *J. Phys. D: Appl. Phys.* **36** R127
[4] Hwang H Y, Cheong S-W, Radaelli P G, Marezio M and Batlogg B 1995 *Phys. Rev. Lett.* **75** 914
[5] Mira J, Rivas J, Hueso L E, Rivadulla F, Quintela M A L, Rodríguez M A S and Ramos C A 2001 *Phys. Rev.* B **65** 024418
[6] Medarde M, Mesot J, Lacorre P, Rosenkranz S, Fischer P and Gobrecht K 1995 *Phys. Rev.* B **52** 9248
[7] Radaelli P G, Iannone G, Marezio M, Hwang H Y, Cheong S-W, Jorgensen J D and Argyriou D N 1997 *Phys. Rev.* B **56** 8265
[8] Ahn K H and Millis A J 2001 *Phys. Rev.* B **64** 115103
[9] Zhao G-M, Conder K, Keller H and Müller K A 1996 *Nature* **381** 676
[10] Chen X J, Soltan S, Zhang H and Habermeier H-U 2002 *Phys. Rev.* B **65** 174402
[11] Kozlenko D P, Glazkov V P, Sadykov R A, Savenko B N, Voronin V I and Medvedeva I V 2003 *J. Magn. Magn. Mater.* **258/259** 290
[12] Millis A J, Darling T and Migliori A 1998 *J. Appl. Phys.* **83** 1588
[13] Tsui F, Smoak M C, Nath T K and Eom C B 2000 *Appl. Phys. Lett.* **76** 2421
[14] Wang H S, Wertz E, Hu Y F and Li Q 2000 *J. Appl. Phys.* **87** 7049
[15] Catlow C R A and Price G D 1990 *Nature* **347** 243
[16] Catlow C R A 1982 *Computer Simulation of Solids* (*Lecture Notes in Physics* vol 166) ed C R A Catlow and W C Mackrodt (Berlin: Springer)
[17] Allan N L, Barrera G D, Fracchia R M, Lavrentiev M Y, Taylor M B, Todorov I T and Purton J A 2001 *Phys. Rev.* B **63** 094203
[18] Isoardi E P, Allan N L and Barrera G D 2004 *Phys. Rev.* B **69** 024303
[19] Allan N L, Barrera G D, Lavrentiev M Y, Todorov I T and Purton J A 2001 *J. Mater. Chem.* **11** 63
[20] Zhang X, Yip K W and Ong C K 1995 *Phys. Rev.* B **51** 1277
[21] Shao Y and Zhang X 2004 *J. Phys.: Condens. Matter* **16** 1103
[22] Zhang X and Catlow C R A 1993 *Phys. Rev.* B **47** 5315
[23] Zhang X and Wang L 2003 *J. Phys. Chem. Solids* **64** 1207
[24] Hébert S, Martin C, Maignan A, Retoux R, Hervieu M, Nguyen N and Raveau B 2002 *Phys. Rev.* B **65** 104420
[25] Toulemonde O, Studer F, Barnabé A, Maignan A, Martin C and Raveau B 1998 *Eur. Phys. J.* B **4** 159
[26] Toulemonde O, Studer F and Raveau B 2001 *Solid State Commun.* **118** 107
[27] Autret C, Hejtmánek J, Knížek K, Maryško M, Jirák Z, Dlouhá M and Vratislav S 2005 *J. Phys.: Condens. Matter* **17** 1601
[28] Sánchez M C, García J, Blasco J, Subías G and Perez-Cacho J 2002 *Phys. Rev.* B **65** 144409
[29] Gilleo M A 1957 *Acta Crystallogr.* **10** 161
[30] Rodríguez-Carvajal J, Hennion M, Moussa F, Moudden A H, Pinsard L and Revcolevschi A 1998 *Phys. Rev.* B **57** R3189
[31] García-Muñoz J L, Suaaidi M and Fontcuberta J 1997 *Phys. Rev.* B **55** 34
[32] Yaicle C *et al* 2003 *Phys. Rev.* B **68** 224412
[33] Sawada H, Morikawa Y, Terakura K and Hamada N 1997 *Phys. Rev.* B **56** 12154
[34] Fita I M, Szymczak R, Baran M, Markovich V, Puzniak R, Wisniewski A, Shiryaev S V, Varyukhin V N and Szymczak H 2003 *Phys. Rev.* B **68** 014436
[35] Ramakrishnan T V, Krishnamurthy H R, Hassan S R and Pai G V 2004 *Phys. Rev. Lett.* **92** 157203
[36] Yamamoto A and Oda K 2002 *J. Phys.: Condens. Matter* **14** 1075
[37] Troyanchuk I O, Lobanovsky L S, Khalyavin D D, Pastushonok S N and Szymczak H 2000 *J. Magn. Magn. Mater.* **210** 63
[38] Joly V L J, Joy P A and Date S K 2001 *J. Phys.: Condens. Matter* **13** L841